IR characterization of $Ln_{2-x}Sr_xCoO_4$ ($x \geq 1$; Ln=La, Nd) oxides

S. Castro-García [a], M. Sánchez-Andújar[a], C. Rey-Cabezudo[a], M.A. Señarís-Rodríguez[a], C. Julien[b]

[a] Dpto. Química Fundamental, Universidad de A Coruña, 15071 A Coruña, Spain

[b] LMDH, Université Pierre et Marie Curie, 4 place Jussieu, 75252 Paris, France

Journal of Alloys and Compounds

Volumes 323–324, 12 July 2001, Pages 710–713

Proceedings of the 4th International Conference on f-Elements

Available online 25 June 2001

doi:10.1016/S0925-8388(01)01049-0

Abstract

We have recorded the FTIR spectra of powder samples of $Ln_{2-x}Sr_xCoO_4$ (Ln=La, Nd) at room temperature. We have identified the infrared active modes ($3A_{2u}+4E_u$), and analyzed how they change as a function of Ln and the Sr doping. We correlate the obtained results with structural data obtained from powder X-ray diffraction studies and with the electronic properties displayed by these samples.

Keywords

Magnetically ordered materials; Chemical synthesis; Crystal structure and symmetry; Phonons; Light absorption and reflection

1. Introduction

$Ln_{2-x}Sr_xCoO_4$ oxides (Ln=La, Nd) are systems that crystallize in the K_2NiF_4-type structure (Fig. 1), that is the 2D analogue of the perovskite type [1]. Their structure has been described as a sequence of tetragonally distorted [CoO_6] octahedra, the Ln^{3+} and Sr^{2+} ions being located in 9-coordinated sites between the layers. These compounds are closely related to $Ln_{1-x}Sr_xCoO_{3-\delta}$ perovskite materials [2], [3],[4], [5], [6], [7], [8] and [9], that have attracted a lot of attention in view of how their magnetic and electrical properties can be varied by changing the rare earth [4], [5] and [7] and the degree of Sr-doping [3] and [6]. Nevertheless $Ln_{2-x}Sr_xCoO_4$ (with $x \geq 1$) compounds have been relatively less studied, probably due to the difficulty to synthesize them and to stabilize the Co^{3+}, Co^{4+} formal states in the K_2NiF_4 structure. The magnetic and electrical properties of the $Ln_{2-x}Sr_xCoO_4$ also change with x [10] and [11]: their electrical resistivity decreases as x increases, even if the metallic regime is not achieved; also, a ferromagnetic contribution starts to develop for $x>1.2$ at $T \leq 175$ K even if to a lesser extend than in the corresponding $Ln_{2-x}Sr_xCoO_{3-\delta}$ materials.

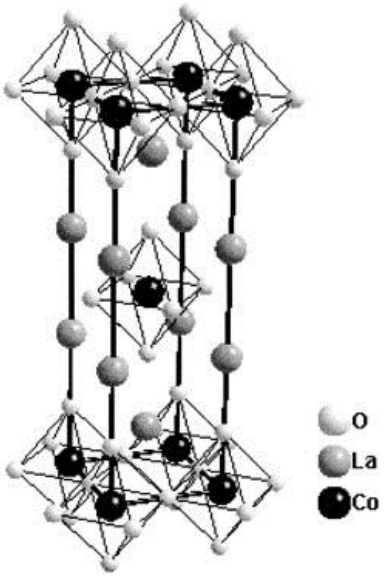

Fig. 1.
The K_2NiF_4-type structure.

To get more information about these relatively poorly characterized $Ln_{2-x}Sr_xCoO_4$ materials, we have studied them by means of powder X-ray diffraction and IR spectroscopy. In this paper we present and discuss the results obtained for Ln=La and Nd with $1.0 \leq x \leq 1.4$ and $1.0 \leq x \leq 1.3$, respectively.

2. Experimental

Samples of $La_{2-x}Sr_xCoO_4$ ($1.0 \leq x \leq 1.4$) and of $Nd_{2-x}Sr_xCoO_4$ ($1 \leq x \leq 1.3$) were prepared by a nitrate decomposition method. Stoichiometric quantities of La_2O_3/Nd_2O_3, $SrCO_3$ were dissolved in HNO_3 (30%) followed by the addition of stoichiometric amounts of $Co(NO_3)_2 \cdot 6H_2O$. The resulting solution was gently warmed up so as to slowly evaporate the solvent. To facilitate the formation of highly oxidized samples, a melting agent, KNO_3, was then added to the so-obtained mixture of nitrates, in a mole ratio 1 KNO_3:1 $Co(NO_3)_2 \cdot 6H_2O$. This mixture was then treated in air at 400°C for 1 h, 600°C for 48 h, and 975°C for 24 h with intermediate grinding after each heating step. X-ray powder diffraction measurements were carried out with a Siemens D-5000 diffractometer and CuK_α=1.5418 Å radiation. Semiquantitative EDAX analysis was carried out in a scanning electron microscope (model JEOL 6400) at 40 kV. FTIR absorption spectra were recorded at room temperature using an interferometer (Brucker model IFS113v) equipped with a 3.5-μm-thick beamsplitter, a global source, and a DTGS/PE far-infrared detector. Samples were ground to fine powders into ICs pellets. Data were collected in transmission mode at a spectral resolution of 2 cm^{-1} after 256 scans in vacuum atmosphere.

3. Results and discussion

3.1. XRD characterization

According to their XRD patterns, all compounds were obtained as single-phase crystalline materials and were K^+-free, as shown by EDAX analysis. This means that a complete solid solution between Ln and Sr can be formed in $Ln_{2-x}Sr_xCoO_4$ in the range $1 \leq x \leq 1.4$ for Ln=La and $1 \leq x \leq 1.3$ for Ln=Nd. These compounds crystallize in the K_2NiF_4 structure, that is body-centered tetragonal, space group *I4/mmm* with Z=2. This structure can be thought to consist of a perovskite layer separated by a rock-salt type $(Ln,Sr)_2O_2$ layer along *c*-axis. The cobalt atoms are located at the *2a* site, the (La or Nd)/Sr randomly occupy the *4e* site. There are two types of oxygen atoms, O(*4c*) located in the *ab* planes and O(*4e*) located in the $(Ln,Sr)_2O_2$block above and below the cobalt atoms. Consequently, the cobalt atoms are in a distorted octahedral environment, where there are two different Co–O bonds: an axial Co–O(I) bond (in the *ab* plane) shorter than the apical Co–O(II) bond (along the *c* direction).

Fig. 2a and b show the variation of the lattice parameters and the cell volume as a function of *x* in $Ln_{2-x}Sr_xCoO_4$ compounds for Ln=La and Nd. As it can be observed in these figures, in both series the *c*parameter clearly increases with doping, whereas the *a* parameter changes very slightly. The cell volume in $Nd_{2-x}Sr_xCoO_4$ series increases with Sr content. In the $La_{2-x}Sr_xCoO_4$ system the same trend is observed when *x* is small, but for *x*>1.2 it remains almost constant. To explain these variations we need to take into account that when Ln is substituted by Sr, a larger size Sr^{+2} ion ($^{IX}r_{Sr+2}$=1.30 Å) is incorporated in place of smaller size Ln^{3+} ion ($^{IX}r_{Nd3+}$=1.16 Å, $^{IX}r_{La+3}$=1.216 Å) [12]. On the other hand, upon doping Co^{3+} ($^{VI}r_{Co3+(l.s.)}$=0.55 Å, $^{VI}r_{CoIII+(h.s.)}$=0.61 Å) oxidates to the smaller Co^{4+} ions ($^{VI}r_{Co4+(h.s.)}$=0.53 Å) [12]. In the case of the Nd-cobaltites, where there is a bigger size difference between Ln^{3+} and Sr^{2+}, the former factor predominates, so that the cell volume and the *c* parameter are seeing to increase with *x*. Nevertheless, in the case of the La-cobaltites where the size difference between La^{3+} and Sr^{2+} is relatively smaller the former factor dominates only for small *x* (*x*<1.2). For higher *x*, the two factors — that work in opposite directions — are balanced, their effect gets cancelled and neither the volume nor the *c* parameter change upon further doping.

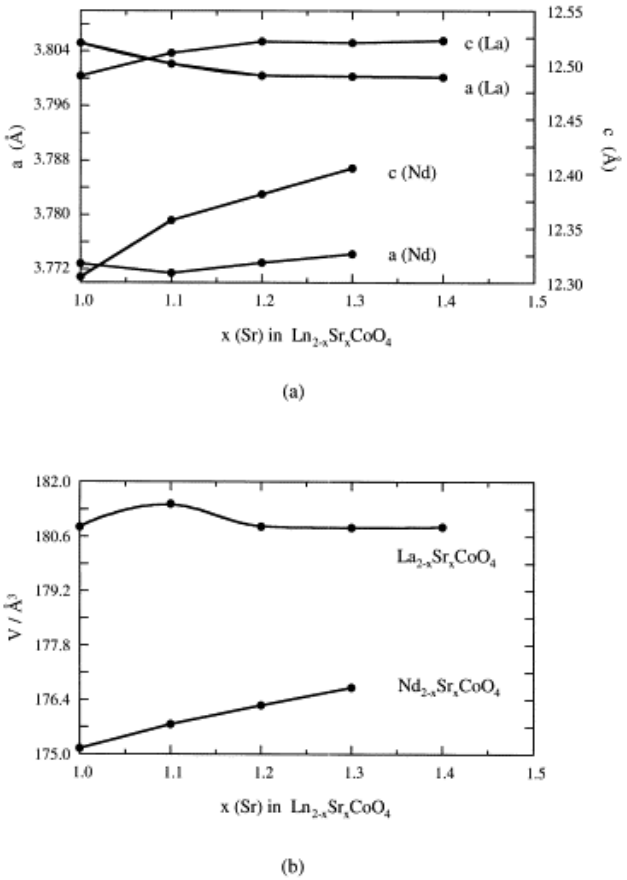

Fig. 2.

Evolution of (a) the lattice parameters and (b) the cell volume as a function of *x* in $Ln_{2-x}Sr_xCoO_4$ compounds with Ln=La and Nd

It should be noted that small differences in structural parameters such as Co–O distances and the degree of distortion of the [CoO_6] octahedra are observed among the La and Nd series of compounds. In this context, Table 1 gives the Co–O(I) and Co–O(II) distances corresponding to $LnSrCoO_4$ compounds (Ln=La and Nd) calculated by Rietveld analysis.

Table 1.

Co–O distances in $LaSrCoO_4$ and $NdSrCoO_4$ compounds as obtained from XRD Rietveld analysis. d(Co–O(I)) corresponds to the axial bond in the *ab* plane while the d(Co–O(II)) corresponds to the apical bond along the *c* direction

Compound	d(Co–O(I)) (Å)	d(Co–O(II)) (Å)
$LaSrCoO_4$	1.9026	2.0374
$NdSrCoO_4$	1.8864	2.0135

3.2. FTIR characterization

The factor group analysis of the K_2NiF_4 structure with *I4/mmm* (D_{4h}^{17}) space group indicates that there are seven infrared-active modes ($3A_{2u}+4E_u$) and three Raman-active modes; we can describe them following the interpretation of Daturi et al. [13] for Nd_2CuO_4 compounds that distinguishes 'internal' vibrations of the $[CuO_2]_n$ sheets, from internal vibrations of the $[Nd_2O_2]_n$ blocks and the lattice vibrations of these two units.

Fig. 3a and b show the FTIR spectra that we obtain for $Ln_{2-x}Sr_xCoO_4$ compounds (Ln=La and Nd, respectively) that are quite similar to those shown by other oxides with K_2NiF_4 structure [14] and [15], andTable 2 and Table 3 list the IR bands observed together with their assignment. Taking into account that powder morphology can affect these spectra [16], the position of the observed bands do not correspond to the transverse optical (TO) modes but are more or less shifted towards the longitudinal optical (LO) modes. Despite the fact that the LO–TO splitting can be large in oxide compounds, the phonon values have been evaluated from absorption experiments on powdered samples, for which FTIR reflectivity can not be accurately measured.

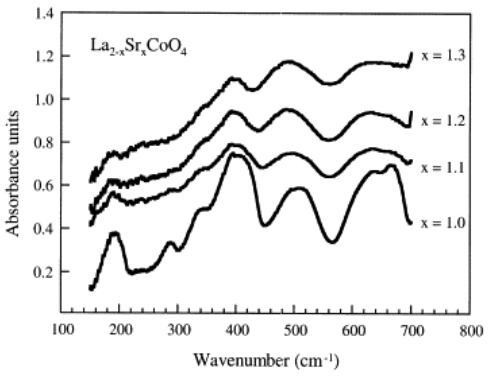

(a)

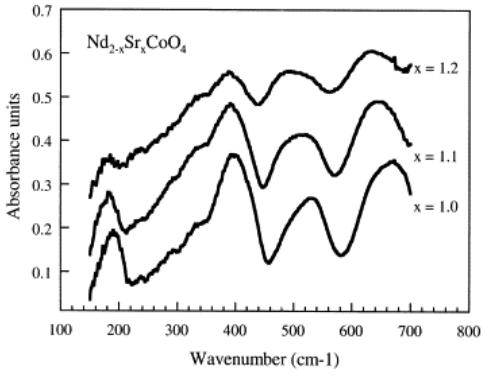

(b)

Fig. 3.

FTIR spectra of $Ln_{2-}xSrxCoO_4$ compounds (Ln=La, Nd). The IR spectra have been vertically shifted according to their *x* content so that they can be easily seen.

Table 2.

Wavenumber (cm^{-1}) and assignment of the IR bands of the $LaSrCoO_4$ and $NdSrCoO_4$ compounds

Symmetry	*v*($LaSrCoO_4$)	*v*($NdSrCoO_4$)	Assignment
E_u	670,640	666	Asymmetric Co−O(I)−Co stretching in
			the *ab* plane
A_{2u}	510	528	Out of plane Co−O(I)−Co deformation
E_u	400	397	In plane Co−O(I)−Co deformation
A_{2u}	350	344	Deformations of (La or Nd)/Sr−O(II)
E_u	290	293	Stretching of (La or Nd)/Sr−O(II)
A_{2u}	240	237	Lattice mode:
			Motion of Co−O(I)−Co layers against the
			(La or Nd)/Sr−O(II) blocks
E_u	190	190	Lattice mode:
			Sliding of the Co−O layers with respect to
			(La or Nd)/Sr−O(II)

Table 3.

Wavenumber (cm^{-1}) and assignment of the IR bands of the $Ln_{2-x}Sr_xCoO_4$ compounds

Symmetry	$La_{2-x}Sr_xCoO_4$				$Nd_{2-x}Sr_xCoO_4$		
	x=1.0	x=1.1	x=1.2	x=1.3	x=1.0	x=1.1	x=1.2
E_u	670, 640	631	631	631	666	640	627
A_{2u}	510	492	483	483	528	510	492
E_u	400	391	391	391	397	396	389
E_u	189	185	185	185	189	183	180

The first interesting point to note about the FTIR spectra is that in both series of compounds the bands that appear in the high frequency region (v>400 cm^{-1}) correspond to modes related to Co–O stretching and deformations; the bands that appear in the range 250<v<400 cm^{-1} correspond to modes related to (Ln,Sr)–O vibrations and those appearing at v<250 cm^{-1} correspond to modes related to lattice modes.

If we compare the spectra of the $LaSrCoO_4$ with those of the corresponding $NdSrCoO_4$ compound, we can give a mere estimation on the frequency shift due to the mass and Co–O distances changes, taking into account that the vibration energy is proportional to the square root of the bond strength and inversely to the square root of the atomic mass. We observe a slight frequency shift of the Co–O deformation modes due to the shorter bonding distances in $NdSrCoO_4$ (Table 1). As $LaSrCoO_4$ are lighter than $NdSrCoO_4$ we observe a frequency shift of the A_{2u} mode (corresponding to the deformations of the Ln, Sr–O bonds) from 344 to 350 cm^{-1} which is in good accordance with the mass change.

If we compare how the spectra change as a function of x in a given $Ln_{2-x}Sr_xCoO_4$ series, the most remarkable feature is an increasing screening effect of the in-plane *ab* modes (see Fig. 3). This effect can be explained on the basis that upon doping charge carriers are created, resulting in an increase of the bidimensional conductivity of the $[CoO_2]_n$ sheets, as corroborated in fact by means of electrical conductivity measurements [17]. Nevertheless, none of these systems achieves the metallic regime in the compositional studied range.

For Nd-cobaltites, the Sr doping induces an increasing unit cell volume with higher Co–O distances. This results in the lowering of FTIR frequencies. For La-cobaltites we observe two different behaviors: (1) for 1.0≤x≤1.1, a larger unit-cell volume with higher

Co–O distances is observed, resulting in a lowering FTIR frequencies and (2) for $1.1 \leq x \leq 1.3$, we do not observe any variations in both the lattice parameters and FTIR mode frequencies.

References

1. S.N. Ruddlesden, P. Popper
   Acta Crystallogr., 10 (1957), p. 538

2. P.M. Raccah, J.B. Goodenough
   J. Appl. Phys., 39 (1968), p. 1209

3. M.A. Señarís-Rodríguez, J.B. Goodenough
   J. Solid State Chem., 116 (1995), p. 224

4. C.N.R. Rao, O.M. Parkash, D. Bahadur, P. Ganguly, A. Nagabhu Share
   J. Solid State Chem., 22 (1977), p. 353

5. G. Demazeau, M. Pouchard, P. Hagenmuller
   J. Solid State Chem., 9 (1974), p. 202

6. M. Itoh, I. Natori, S. Kubota, K. Matoya
   J. Phys. Soc. Jpn., 63 (1994), p. 1486

7. C.N.R. Rao, O.M. Parkash
   Phil. Mag., 35 (1977), p. 1111

8. M.P. Breijo, C. Rey, S. Castro, M. Sánchez, M.A. Señarís-Rodriguez, J. Mira, A. Fondado, J. Rivas
   Ionics, 4 (1998), p. 267

9. M.A. Señarís-Rodriguez, M.P. Breijo, S. Castro, C. Rey, M. Sanchez, R.D. Sanchez, J. Mira, A. Fondado, J. Rivas
   Int. J. Inorg. Mater., 1 (1999), p. 281

10. T. Matsuura, J. Tabuchi, J. Mizusaki, S. Yamauchi, K. Fueki
    J. Phys. Chem. Solids, 49 (1988), p. 1403

11. Y. Moritomo, K. Higashi, K. Matsuda, A. Nakamura
    Phys. Rev. B, 55 (1997), p. 14725

12. R.D. Shannon, C.T. Prewitt
    Acta Crystallogr., A32 (1976), p. 751

13. M. Daturi, G. Busca, E. Magnone, M. Ferretti
    J. Solid State Chem., 119 (1995), p. 36

14. M.K. Crawford, G. Burns, E.M. MacCarron III, R.J. Smalley
    Phys. Rev. B, 41 (1990), p. 8933

15. F. Gervais, P. Echegut, J.M. Bassat, P. Odier

Phys. Rev. B, 37 (1988), p. 9364

16. S. Hayashi, N. Nakamori, J. Hirono, H. Kanamori
J. Phys. Soc. Jpn., 43 (1977), p. 2006

17. M. Sánchez-Andújar and M.A. Señarís-Rodríguez, to be published.

Corresponding author. Tel.: +34-981-167-000; fax: +34-981-167-065 suquie@udc.es